Hierarchical Nanostructures of Bent-Core Molecules Blended with Poly(styrene-*b*-4-vinylpyridine) Block Copolymer

Kishore K. Tenneti,[†] Xiaofang Chen,[†,‡] Christopher Y. Li,*[,†] Xinhua Wan,[‡] Xinhe Fan,[‡] Qi-Feng Zhou,*[,‡] Lixia Rong,[§] and Benjamin S. Hsiao[§]

A.J. Drexel Nanotechnology Institute and Department of Materials Science and Engineering, Drexel University, Philadelphia, Pennsylvania 19104; Department of Polymer Science and Engineering and The Key Laboratory of Polymer Chemistry and Physics of Ministry of Education, College of Chemistry, Peking University, Beijing 100871, P. R. China; and Department of Chemistry, Stony Brook University, Stony Brook, New York 11794

Received March 24, 2007; Revised Manuscript Received May 6, 2007

ABSTRACT: We report the phase structures observed in blends of poly(styrene-*b*-4-vinylpyridine) (PS-*b*-P4VP) block copolymer (BCP) and a bent-core molecule 1-[4′-(3″,4″,5″-tridecyloxybenzoyloxy)phenyleneoxycarbonyl]-3-[(4′-hydroxyphenyl)oxycarbonyl]benzene (BP). Hydrogen bonding between the terminal −OH group of BP and pyridine of P4VP led to the formation of P4VP(BP)$_n$ complex, which exhibited liquid crystalline (LC) order. This LC ordering, combined with microphase separation of the BCP, led to the formation of hierarchical nanostructures. The phase structures of the blend samples were investigated as a function of the concentration of BP using small-angle and wide-angle X-ray scattering and transmission electron microscopy techniques. By increasing the BP content, BCP phase morphology transformed from lamellae to cylinders. In the two cases investigated, the P4VP/BP complex formed a bilayer smectic A LC structure within the BCP domains, and these layered structures were oriented perpendicular to the BCP interface. A detailed structural and morphological study will be reported.

Introduction

Hierarchical nanostructures, usually spanning from the molecular scale (sub-nanometers) to hundreds of nanometers, are of great technological importance. Block copolymers (BCPs) provide one of the most straightforward templates to achieve hierarchical nanostrucutres.[1] BCP microphase separation could lead to the formation of a variety of structures such as lamellae, cylinders, gyroid, and spheres.[2] The length scale of these phase separated structures is ∼10−50 nm. Amorphous BCP (coil−coil) phase structures have been extensively investigated.[2,3] Tuning the chemical structure of one or several segments of the BCP leads to the possibility of forming a secondary structural order within the BCP domains. To this end, a few types of BCP systems have been proposed, including crystalline−amorphous (or crystalline−crystalline) BCPs[4−8] and liquid crystalline (LC) BCPs.[9−20] In the first case, polymer chains crystallize in the confined (soft or hard confinement) space that is formed by the BCP microphase separation. Structural hierarchy can be achieved due to the ordered structure formation at two different length scales as a result of BCP microphase separation (10−50 nm) and the crystalline structure formation (1−10 nm). In the second case, LC or LC polymers are used as one BCP block. LCs form ordered structures on the 1−10 nm length scale. Thus, LC BCPs represent a natural hierarchical-structure-forming system. The structural flexibility of LC also enables incorporating functionalities into BCP microdomains. A number of LC BCPs have been investigated. Depending on the LC molecular architecture, LC BCPs can be divided into side-chain LC−BCPs,[9,12−14,20] main-chain LC−BCP,[15,16] and BCPs formed by mesogen-jacketed LCs.[17,18] In these systems, the liquid crystallinity of the mesogen played an important role in the evolution of overall BCP structure. Both conventional and nonconventional morphologies have been reported in LC BCPs. Soft spacers were introduced between the polymer main chain and the end of the mesogens, resulting in side-chain LC BCPs. Increased mobility of the chains led to the formation of conventional BCP morphologies combined with LC ordering.[13,14,20] A number of research groups have also reported unique phase structures formed in the rod−coil BCP systems which combine two blocks with extreme chain conformations (rigid and flexible).[11,15,17−19] In recent years, a lot of research is focused on the development of BCP supramolecular structures (formed between BCP and a low molar mass moiety) based on noncovalent interactions such as ionic interactions,[21−23] metal coordinate complex formation,[24−26] and hydrogen bonding.[27−31] In general, these interactions between a polymer and a low molar mass substance lead to the formation of phase-separated structures in the range of 1−5 nm. By introducing such polymer/moiety complexes as one BCP block, hierarchical structure-in-structure morphologies have been achieved. Designing supramolecular dynamic and functional materials based on these weaker bonds is an attractive area of research because of the ease with which complex architectures can be formed and deformed as necessary. Using solvent extraction, the small molar mass moiety can also be dissolved, leading to the formation of nanoporous films.[30] Deposition of metals in such nanopores leads to the formation of arrays of nanodots and nanowires.[31]

Hydrogen bonding has been extensively used to create LC structures. Kato et al. reported the formation of supramolecular LC materials using H-bonding. Small molecules with an end-functional group form hydrogen bond with polymers such as poly(vinylpyridine). In these systems, LC ordering was induced in nonmesogenic molecules due to the H-bond, and these complexes exhibited thermotropic nematic and smectic LC

* Corresponding authors. Christopher Li: Ph 215-895-2083, Fax 215-895-6760, e-mail chrisli@drexel.edu. Qi-Feng Zhou: Ph 86-10-62756660, e-mail qfzhou@pku.edu.cn.
[†] Drexel University.
[‡] Peking University.
[§] Stony Brook University.

10.1021/ma070721j CCC: $37.00
Published on Web 06/12/2007

phases.[32,33] Such systems are attractive candidates for use as stimuli-responsive materials because of the dynamic nature of the weak hydrogen bond. Ikkala and ten Brinke have employed H-bonding to form supramolecular structure-in-structure morphologies in a variety of BCP−amphiphile systems. In one typical system, small molar mass amphiphile nonadecylphenol (NDP) was used in which the phenol end group of NDP forms hydrogen bond with the pyridine of poly(styrene-*b*-4-vinylpyridine) (PS-*b*-P4VP). Microphase separation led to the formation of PS and P4VP−NDP domains, and within the P4VP−NDP domains, the polar and nonpolar segments of NDP underwent phase separation and formed layered structures. NDP lamellar layers were also observed in cylindrical and spherical BCP systems.[29]

In this article, we report unique phase structures formed in a BCP−small molecule complex system, as shown in Scheme 1a. Bent-core 1-[4′-(3″,4″,5″-tridecyloxybenzoyloxy)-phenyleneoxycarbonyl]-3-[(4′-hydroxyphenyl)oxycarbonyl]-benzene ($BP_{10/3}$-OH, 3 denotes three alkyl tails per mesogen, and 10 stands for the number of carbon atoms in each tail; we shall use BP in the following text since this is the only H-bond-forming small molecule we will use in this article) molecule with hydroxyl end group as the proton donor forms hydrogen-bonded complex with the pyridine group of poly(styrene-*b*-4-vinylpyridine) (PS-*b*-P4VP) BCP. Bent-core (also known as banana/bow) molecules have drawn considerable attention recently because they exhibit interesting phase structures and excellent electro-optical properties.[34−40] In our system, the bent core in the molecule is achieved by substituting on the 3- and 5-positions of the central benzene ring. PS and P4VP−BP blocks undergo phase separation and form ordered structures (10−100 nm) whose morphology depends on the weight fraction of the blocks. The polar and nonpolar segments of P4VP−BP complex further undergo phase separation and form unique LC smectic layers (1−10 nm) in P4VP domain of the BCP, resulting in a structure-in-structure type of morphology. Small-angle X-ray scattering (SAXS), wide-angle X-ray diffraction (WAXD), and transmission electron microscopy (TEM) results will be presented, and the phase structures of the BCP−BP complexes will be discussed.

Experimental Section

Materials. 4-(Dimethylamino)pyridine (DMAP, 99%) was used as received from Acros. Isophthalic acid (99%), *N*,*N*′-dicyclohexylcarbodiimide (DCC, 95%), and palladium carbon catalyst were used as received from Beijing Chemical Co. 1,4-Dioxaxne (99%), 4-benzyloxyphenyl (99%), dichloromethane (99.5%), 3,4,5-trihydroxybenzoic acid methyl ester (98%), 1-bromodecane (98%), K_2CO_3, KOH, ethanol (99.5%), ethyl acetate (99.8%), acetone (99.9%), and dichloromethane (99.5%) were used as received from Sigma-Aldrich. Tetrahydrofuran (99.9%) (THF) was also purchased from Sigma-Aldrich and was refluxed over sodium under argon and distilled out before use. Diblock copolymer of polystyrene and poly(4-vinylpyridine), PS_{115}-*b*-$P4VP_{112}$ (weight-average molecular weight, $M_w = 23\,800$, $M_w/M_n = 1.03$, where M_n is the number-average molecular weight), was purchased from Polymer Source Inc. and was used without purification.

Synthesis of 1-[4′-(3″,4″,5″-Tridecyloxybenzoyloxy)phenyleneoxycarbonyl]-3-[(4′-hydroxyphenyl)oxycarbonyl]benzene ($BP_{10/3}$-OH) The synthetic procedure of BP is shown in Scheme 1b.

1,3-Bis[(4-hydroxyphenyl)oxycarbonyl]benzene (1). 4-Benzyloxyphenol (10.01 g, 50 mmol), isophthalic acid (4.15 g, 25 mmol), DMAP (0.61 g, 5 mmol), and DCC (10.32 g, 50 mmol) were dissolved in dichloromethane (250 mL). The solution was stirred at room temperature for 3 h. The precipitated *N*,*N*′-dicyclohexylurea was filtered off and washed with dichloromethane for several times.

Scheme 1. (a) Hydrogen Bond Formation between PS-*b*-P4VP and BP, (b) Synthetic Route of 1-[4′-(3″,4″,5″-Tridecyloxybenzoyloxy)phenyleneoxycarbonyl]-3-[(4′-hydroxyphenyl)oxycarbonyl]benzene ($BP_{10/3}$-OH), and (c) ^{1}H NMR Spectra of $BP_{10/3}$-OH

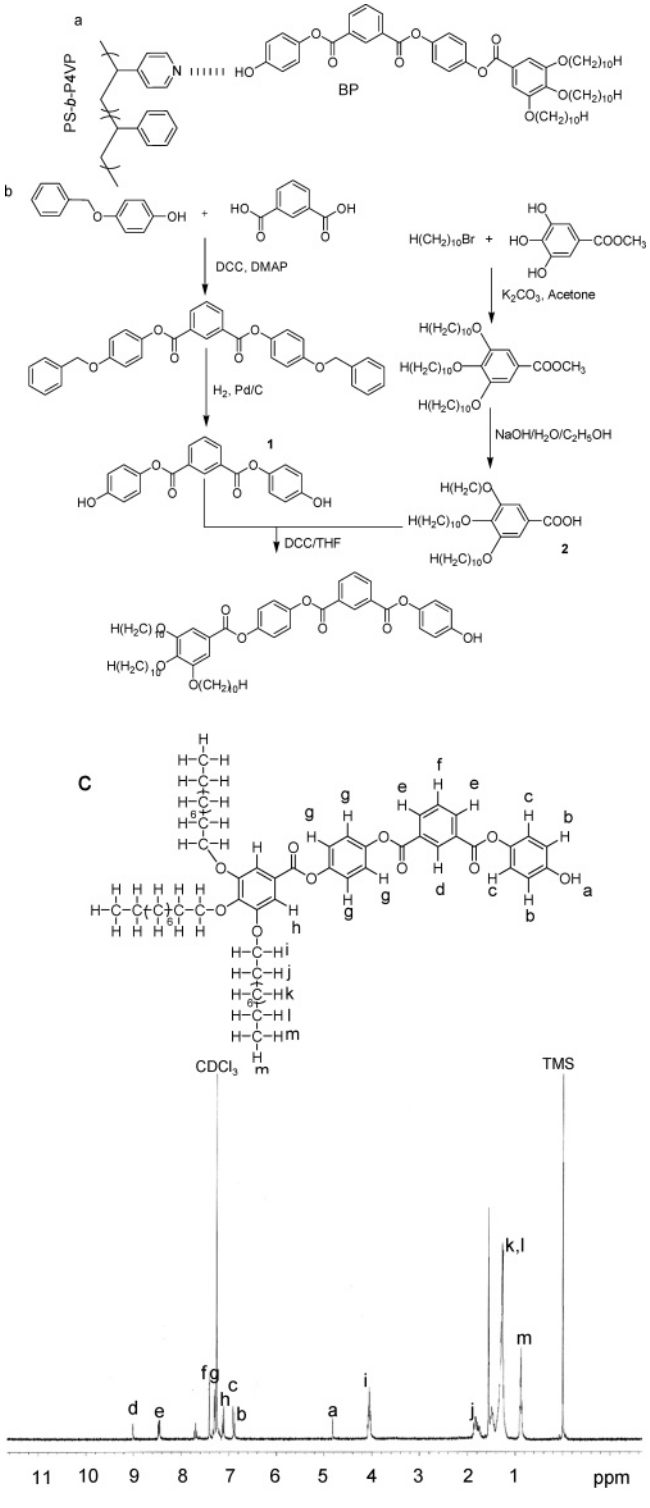

After evaporation of the solvent, the residue was purified by silica gel column chromatography with dichloromethane as the eluent to yield 11.94 g (90%) of product as a white solid. The obtained product was dissolved in 1,4-dioxane (200 mL). 5% Pd/C catalyst (0.6 g) was then added to this solution. The reaction mixture was stirred at 50 °C in hydrogen atmosphere for 5 h. The catalyst was filtered off, and the solvent was removed from the filtrate under reduced pressure. The obtained residue was purified by recrystallization from 1,4-dioxane to yield 6.31 g (80%) of **1** as white

Scheme 2. Schematic Representation of the Shear Geometry

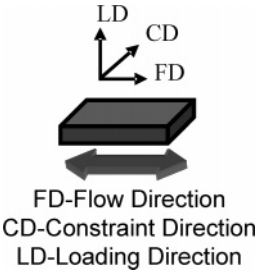

crystals. ^{1}H NMR (δ, ppm, d_6-DMSO): 6.82−6.85 (d, 2H, Ar−*H*), 7.11−7.14 (d, 2H, Ar−*H*), 7.84−7.86 (m, 1H, Ar−*H*), 8.42−8.45 (m, 1H, Ar−*H*), 8.75 (s, 1H, Ar−*H*), 9.55 (s, 2H, −O*H*).

3,4,5-Tris(decyloxy)benzoic Acid (2). 3,4,5-Trihydroxybenzoic acid methyl ester (1.84 g, 10 mmol), 1-bromodecane (7.74 g, 35 mmol), and K_2CO_3 (9.67 g, 70 mmol) were dissolved in acetone (250 mL). The solution was refluxed overnight, and the mixture was poured in water. After adjusting the pH (∼4), the product was extracted using ethyl acetate. The solvent was evaporated, and the product was recrystallized in methanol. This recrystallized product (5.44 g, 9 mmol) and KOH (2.524 g, 45 mmol) were added to ethanol/water solution and refluxed for 1 day. The solution was poured into water, adjusted the pH (∼4), and extracted using ethyl acetate. The solvent was then evaporated, and the residue was purified by recrystallization using methanol to give 4.62 g (87%) of **2**. ^{1}H NMR (δ, ppm, $CDCl_3$): 0.86−0.90 (t, 9H, 3-CH_3), 1.27−1.49 (m, 42H, 3-CH_2−CH_2−C_7H_{14}−), 1.72−1.86 (m, 6H, 3-O−CH_2−CH_2−), 4.00−4.06 (m, 6H, 3-O−CH_2−), 7.32 (s, 2H, Ar−*H*).

1-[4′-(3″,4″,5″-Tridecyloxybenzoyloxy)phenyleneoxycarbonyl]-3-[(4′-hydroxyphenyl)oxycarbonyl]benzene ($BP_{10/3}$-OH). 1,3-Bis-[(4′-hydroxyphenyl)oxycarbonyl]benzene (1.50 g, 4.28 mmol) (**1**), 3,4,5-tris(decyloxy)benzoic acid (2.53 g, 4.28 mmol) (**2**), DMAP (0.05 g, 0.43 mmol), and DCC (0.88 g, 4.28 mmol) were dissolved in tetrahydrofuran (THF) (50 mL). The solution was stirred at room temperature for 12 h. The precipitated *N*,*N*′-dicyclohexylurea was filtered off and washed with THF several times. After evaporation of the solvent, the residue was purified by silica gel column chromatography with dichloromethane and ethyl acetate as the eluent to yield 1.58 g (40%) of product as a white solid. ^{1}H NMR (δ, ppm, $CDCl_3$): 0.86−0.90 (t, 9H, −CH_3), 1.26−1.51 (m, 42H, −(CH_2)$_7$−), 1.79−1.86 (m, 6H, 3-OCH_2CH_2−), 4.04−4.09 (t, 6H, 3-O−CH_2−), 4.8 (s, 1H, −O*H*), 6.88−6.91 (d, 2H, Ar−*H*), 7.11−7.14 (d, 2H, Ar−*H*), 7.27−7.31 (m, 2H, Ar−*H*), 7.42 (s, 4H, Ar−*H*), 7.70 (m, 1H, Ar−*H*), 8.46−8.49 (d, 2H, Ar−*H*), 9.02 (s, 1H, Ar−*H*). Scheme 1c shows the ^{1}H NMR spectra of $BP_{10/3}$-OH.

Blends Preparation. To obtain the supramolecular assembly, PS-*b*-P4VP and BP were dissolved together in dichloromethane to form ∼5 wt % solution. Two PS−P4VP(BP)$_n$ (*n* is the mole ratio of BP and pyridine) samples were prepared. They had different concentration of BP (n = 0.2 and 0.1). The solution was stirred for 20 min at room temperature and was left overnight. The solvent was then allowed to evaporate slowly for 2 days at room temperature. The resulting blend was further dried under vacuum for 1 day to remove the residual solvent. DSC results showed that the T_g of P4VP block in the blends decreased to ∼120 °C. Good microphase separation was obtained when the samples were annealed at 125 °C for 3 days. To achieve uniform alignment of the microdomains, the microphase-separated samples were subjected to a large-amplitude reciprocating shear at ∼125 °C for ∼40 min. The shear frequency was ∼0.5 Hz, and the shear amplitude was ∼150%. The flow, constraint, and loading directions (FD, CD, and LD, respectively) are shown in Scheme 2. The resulting polymer film was taken out of the shearing apparatus and quenched to room temperature. The samples were then annealed at 125 °C for an additional 24 h to release residual shear stress. The final film thickness was ∼0.2−0.3 mm.

Equipment and Experiments. SAXS, WAXD, and TEM were employed to characterize the structure and morphology of the PS−P4VP(BP)$_n$. Two-dimensional (2-D) SAXS experiments were carried out at the synchrotron X-ray beamline X-27C at the National Synchrotron Light Source in Brookhaven National Laboratory. The zero pixel of the 2-D SAXS pattern was calibrated using silver behenate, with the first-order scattering vector q being 1.076 nm^{-1}. The air scattering for WAXD was subtracted. The X-ray beam spot was ∼0.1 mm in diameter. The X-ray beam was along the FD, CD, and LD of the sample (see Scheme 2). 2-D WAXD patterns were also recorded at room temperature in the same setup with the sample-to-detector distance of ∼15−19 cm.

TEM experiments were conducted on a JEOL 2000FX TEM with an accelerating voltage of 120 kV. A Reichert Ultracut cryo-ultramicrotome was used to microtome the sheared block copolymer sample. Thin sections of the BCP (∼50 nm thick) were obtained at room temperature and collected on TEM grids, followed by staining in RuO_4 vapor for ∼40 min.

Results and Discussion

Pure PS_{115}-*b*-$P4VP_{112}$ has a PS weight fraction of ∼0.5, which suggests that the BCP might have a simple lamellar structure. In order to obtain uniformly aligned microdomains of the microphase-separated BCP, the sample was subjected to reciprocating shear. The shear geometry is shown in Scheme 2. Figure 1a shows the 2D SAXS pattern of PS_{115}-*b*-$P4VP_{112}$ along the FD/LD and CD/LD plane. Scattering peaks with three orders possessing a 1:3:5 ratio are evident from the plot indicating a simple lamellar structure. The *d*-spacing corresponding to the first scattering peak is ∼28.6 nm. The disappearance of even order peaks indicates that PS and P4VP domains have similar dimensions.[41] 50 nm thick sections were obtained by ultramicrotoming the sheared sample. The sections were stained with RuO_4 vapors for 40 min before TEM experiments. Figure 1b shows a TEM micrograph of the BCP exhibiting a lamellar structure with alternating dark (P4VP) and white (PS) regions. The layer spacing measured from the TEM is in agreement with the *d*-spacing obtained from the SAXS pattern.

Phase Structures of PS−P4VP(BP)$_{0.1}$. The effective weight fraction of P4VP(BP) complex in PS−P4VP(BP)$_{0.1}$ blend is 0.65. This weight fraction is on the boundary region between a lamellar and cylindrical morphology for the coil−coil diblock copolymer system.[42] Parts a and b of Figure 2 show the SAXS pattern of the sheared PS−P4VP(BP)$_{0.1}$ where the X-rays are along the CD and FD, respectively, as denoted in Scheme 2. The scattering peaks exhibit seven orders that follow a 1:2:3:4:5:6:7 ratio, implying that the sample possesses a long-range lamellar structure. The diffraction arcs are sharper compared to that of the pure BCP, which indicates that the BCP order was improved upon forming the complex. The scattering peaks of PS−P4VP(BP)$_{0.1}$ have a full width at half-maximum (FWHM of first order peak = 0.021 nm^{-1}) that is half of the FWHM of the pure BCP (0.047 nm^{-1}), as shown in Figure 2c,d. The enhanced ordering is believed to be due to the formation of LC structures within the P4VP domain (see following discussion).

In addition to the BCP lamellar scatterings along the equatorial region, two diffuse arcs are present along the meridian direction. The corresponding *d*-spacing is 6.8 nm, indicating the formation of another structure orthogonal to the BCP layers. The WAXD pattern is shown in Figure 2e. In the wide-angle region, two amorphous scattering halos are evident, and the azimuthal scan of the these amorphous scattering (Figure 2f) indicates their azimuthal angles are perpendicular to the 6.8 nm scattering arc observed in the SAXS experiments. Combining SAXS and WAXD experiments, one can conclude a smectic A (SmA)-type phase was formed in the P4VP domains of the BCP complex, and the smectic layer is perpendicular to the lamellar intermaterial dividing surface (IMDS) of the BCP. Since each

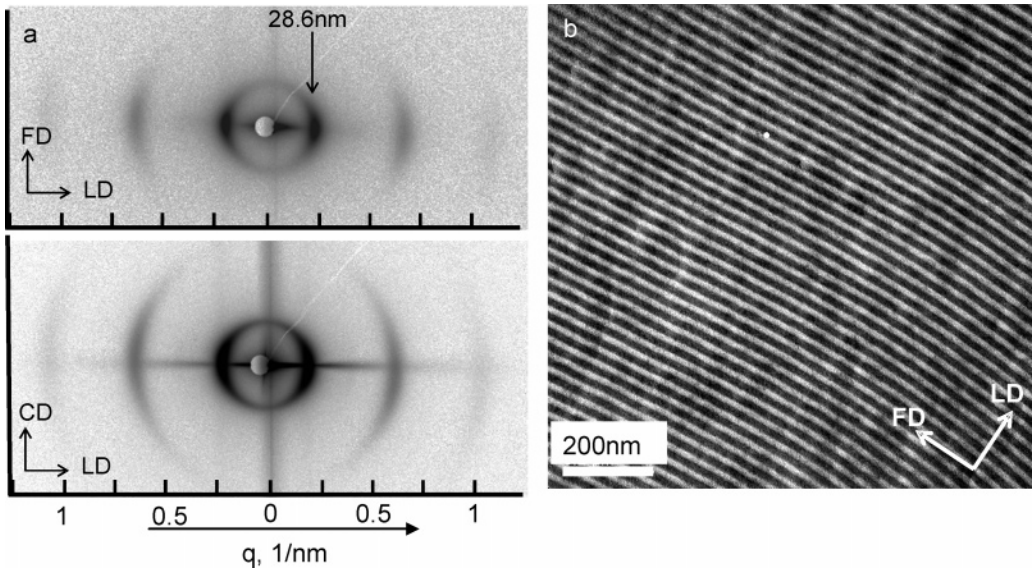

Figure 1. (a) 2D small-angle X-ray scattering pattern of PS_{115}-*b*-$P4VP_{112}$ along the flow/loading direction (FD/LD) and constraint/loading direction (CD/LD) plane. (b) Transmission electron micrograph of PS_{115}-*b*-$P4VP_{112}$ microtomed sample along the FD/LD plane and stained with RuO_4.

BP molecule has a contour length of ~3.3 nm, we propose that each smectic layer consists of two layers of BP molecules forming a bilayer structure (SmA_2), similar to a few other bent-core LC polymers reported.[34,43] The smectic layer scattering arcs are weak, possibly due to the low concentration of the BP molecules. Note that pure BP molecules do not exhibit LC behavior. Therefore, formation of hydrogen bonds between P4VP and BP extended the anisotropy of the BP molecules, which in turn leads to the formation of SmA_2 LC structures.

Figure 3a,b shows the TEM micrographs of PS−P4VP$(BP)_{0.1}$ thin sections along the FD/LD and CD/LD planes. Long-range ordered lamellar structure is evident from the micrograph consisting of dark (P4VP$(BP)_{0.1}$) and white (PS) domains. The inset in Figure 3a shows an enlarged image of the lamellar structure. A similar pattern is also observed along the CD/LD plane. Note that each of the dark P4VP(BP) layer consists of three distinct layers separated by a dark interface. The formation of three distinct layers in one P4VP layer is intriguing. We attribute this to the low content of BP molecules, when $n = 0.1$, only 10% of the P4VP chains formed H-bonds with BP. This led to coexistance of P4VP and P4VP(BP) domains. These two domains are separated into lamellar structure with the P4VP-(BP) layer sandwiched by the P4VP layers, reducing the contact between P4VP(BP) and PS as shown in Figure 4. Alternating dark and light regions represent P4VP(BP) and PS lamellae oriented parallel to the shear direction. Within the P4VP$(BP)_{0.1}$ domains, three distinct regions exist that are separated by a dark interface. The two outer regions consist of P4VP chains, and the inner region is made up of the aggregated BP and P4VP molecules, which are arranged in the form of SmA_2 structures, and the smectic layers are aligned perpendicular to IMDS. Therefore, BCP microphase separation and BP aggregation led to the formation of structure-in-structure type of morphology in the hydrogen-bonded BCP−small molecule system. ten Brinke et al. have performed extensive research on structure-in-structure morphologies observed in BCP−amphiphile systems using a variety of noncovalent interactions including hydrogen bonding, and a number of similar morphologies have been reported.[30−34,36−43,45] In these systems, the small-M_w amphiphile (such as nonadecylphenol and pentadecylphenol) is considered as a solvent in the system and is present in a molar ratio of 1:1 with respect to the P4VP. The uniqueness of our system is that the BP molecule with a long aromatic mesogen readily facilitates smectic layer formation at relatively low blending ratio (as in the case of PS−P4VP$(BP)_{0.1}$). Furthermore, by controlling the BP molecule concentration, three levels of ordering could be formed: (1) BCP phase separation between PS and P4VP/BP, (2) P4VP and P4VP(BP) phase separation in each P4VP-rich layer, and (3) formation of the SmA_2. Also note that, compared to the pure PS_{115}-*b*-$P4VP_{112}$, PS−P4VP$(BP)_{0.1}$ possess a wavy lamellar structure as seen from Figure 3. This might be a result of the cumulative effect of two factors: first, the wavy nature of the smectic layers of the bent-core LCs[35] and, second, the lower content of the BP molecules.

Another interesting feature of our system is the reduction of the lamellar *d*-spacing of the BCP. The *d*-spacing corresponding to the first scattering peak in Figure 2a,b is ~23 nm, which is much smaller than that of the pure PS_{115}-*b*-$P4VP_{112}$ (~28.6 nm). Extensive research has been conducted in the field of BCP/homopolymer blends that emphasize the relation between the BCP domain spacing and the concentration of homopolymer and its M_w.[44−48] In most cases, the domain spacing of BCPs increased with the addition of homopolymers. However, Winey et al. reported that in a polystyrene homopolymer (hPS)/poly-(styrene-*b*-isoprene) (PS-*b*-PI) BCP system low-M_w hPS blends at low concentrations led to an initial decrease in the lamellar *d*-spacing of PS-*b*-PI.[48] It was argued that the increase in the hPS content led to lateral swelling of the PS domains (thus PI chains); hence, the interfacial area increased, which in turn led to a decreased *d*-spacing of the PI domain. In our case, the possible explanation for the decrease in the domain spacing is that within the P4VP$(BP)_{0.1}$ domain the polar and nonpolar domains of the complex underwent phase separation along with the aggregation of BP molecules to form smectic layers. The result of such separation was that the P4VP chains were forced to stretch parallel to the IMDS in order to accommodate the smectic structure formation. This stretching of the P4VP chains along the IMDS led to shrinkage of the chain dimension normal to the IMDS. As a consequence, PS chains also expanded along the IMDS and shrank along the IMDS normal. From the TEM images, it can be observed that in pure PS_{115}-*b*-$P4VP_{112}$ the PS and P4VP domain size is ~14.3 nm each; however, in PS−P4VP$(BP)_{0.1}$, PS domains measure ~10 nm whereas P4VP domains (including three layers) are ~13 nm. This indicates that both PS and P4VP domains are subjected to shrinkage as a result of the BP smectic layer formation.

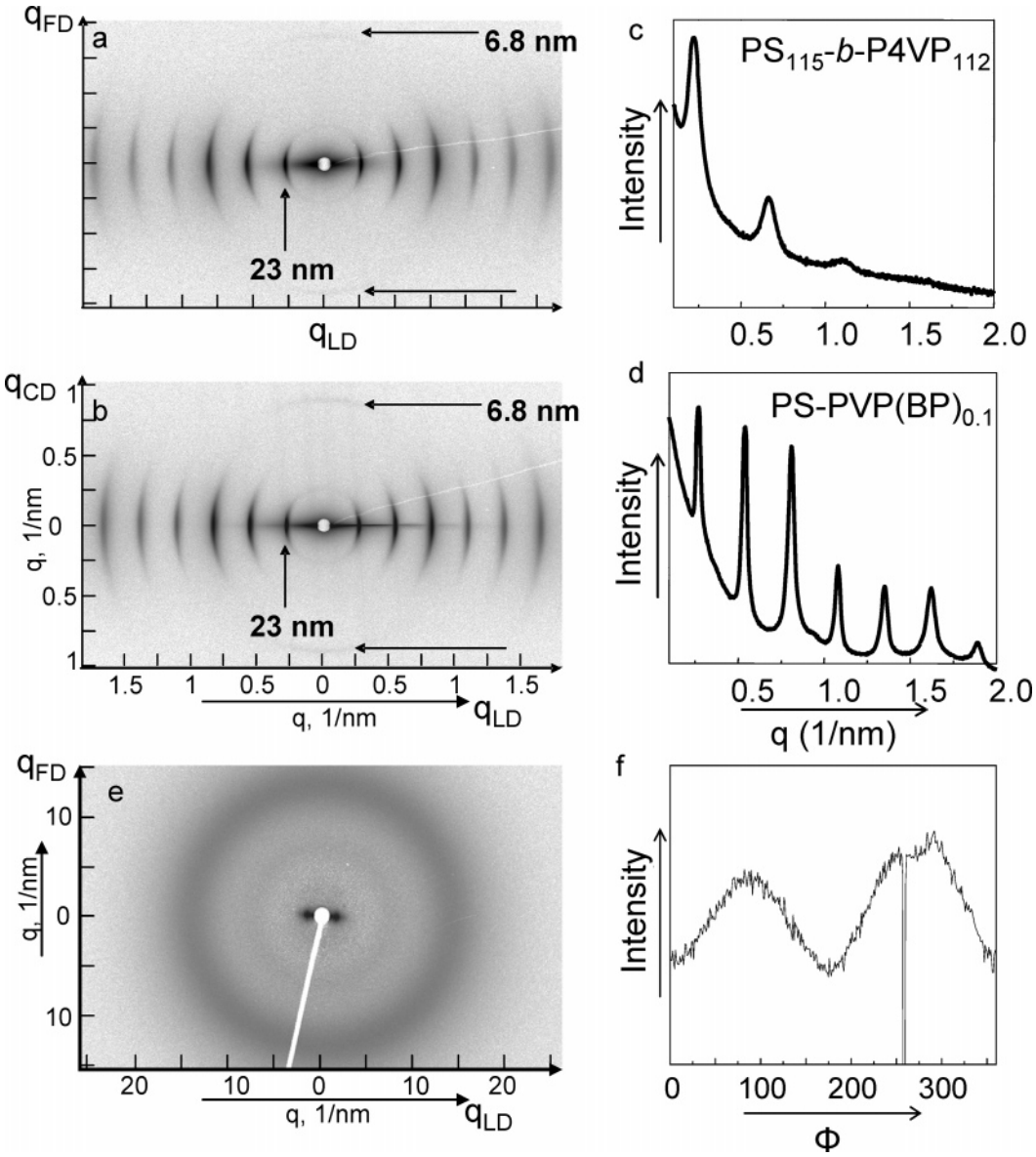

Figure 2. 2D small-angle X-ray scattering pattern of PS−P4VP(BP)$_{0.1}$ with the X-rays along the (a) constraint direction (CD) and (b) flow direction (FD) as defined in Scheme 2. 1D integration of SAXS pattern of (c) pure PS_{115}-*b*-$P4VP_{112}$ and (d) PS−P4VP(BP)$_{0.1}$. (e) Wide-angle X-ray scattering pattern of PS−P4VP(BP)$_{0.1}$ with the X-rays along CD. (f) Azimuthal scan of the amorphous region of (e).

Phase Structures of PS−P4VP(BP)$_{0.2}$. Increasing the concentration of the LC molecules, so that the ratio of the number of pyridine to the number of LC molecules would be 5:1, resulted in the blend PS−P4VP(BP)$_{0.2}$ where the cumulative weight fraction of P4VP(BP)$_{0.2}$ is 0.73. Figure 5a,b shows the 2D X-ray scattering obtained when the X-ray is along the CD and FD of the sample as defined in Scheme 2. In this sample, the scattering peaks due to the BCP ordering are located along the meridian in both the FD/LD and CD/LD planes. These peaks possess a ratio of 1:$\sqrt{3}$:$\sqrt{7}$, suggesting a hexagonally packed cylinder structure. Along the equator, two strong scattering peaks obeying a ratio of 1:2, representative of a layered structure, and having a layer spacing of ~6.8 nm can be clearly observed. These scattering peaks are similar to the SmA_2 that were observed in P4VP(BP)$_{0.1}$ and are oriented perpendicular to the BCP ordering. Figure 5c shows the SAXS pattern obtained along the FD/CD plane of the sample. A scattering pattern with 6-fold symmetry, representative of a hexagonal close packed cylinder structure, is evident from this Figure. On the basis of weight fraction, the P4VP(BP)$_{0.2}$ domain forms the matrix and PS forms the cylindrical phase. Two interesting features are evident from the X-ray results. First, the long axis of the PS cylinders are oriented parallel to the LD. Second, the SmA_2 scattering peaks oriented orthogonal to the BCP ordering are much stronger in intensity compared to those observed in sample P4VP(BP)$_{0.1}$. This might be due to the fact that increased BP concentration leads to the formation of more ordered smectic LC layers. A real-space image of the sample was obtained from TEM of microtomed sections stained with RuO_4. Figure 6a,b shows the TEM micrographs of the samples along the FD/LD and CD/LD planes. Alternate dark and white regions, representing P4VP(BP)$_{0.2}$ and PS domains, respectively, are clearly visible in the figure. Each dark region further contains white strips oriented perpendicular to the BCP interface. These perpendicular domains are uniform and span the entire dark region. Since P4VP domains are preferentially stained by RuO_4, the appearance of the white strips within the P4VP domains indicates that these domains are due to the formation of SmA_2 LC layers, which are oriented normal to the BCP interface as observed from the SAXS experiments. Figure 6c shows the TEM micrograph of

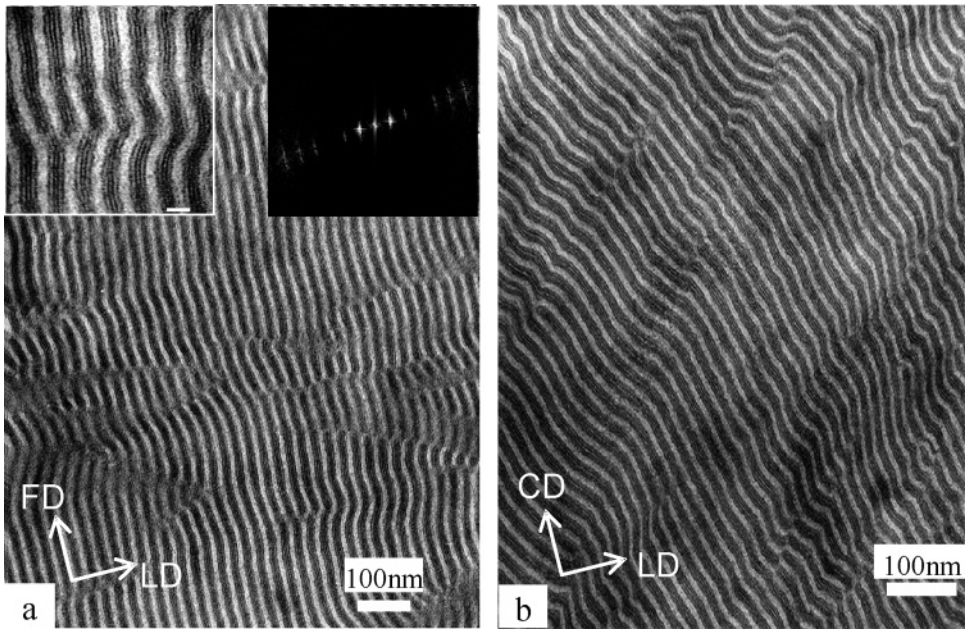

Figure 3. Transmission electron micrograph of PS−P4VP(BP)$_{0.1}$ showing the (a) flow/loading direction (FD/LD) plane. (Inset on the left is magnified image of the lamellar structures which clearly shows that the P4VP(BP)$_{0.1}$ region (dark) is divided into three regions. Inset on the right is the fast Fourier transform of the image, which is similar to the SAXS pattern.) (b) Constraint/loading direction (CD/LD) plane.

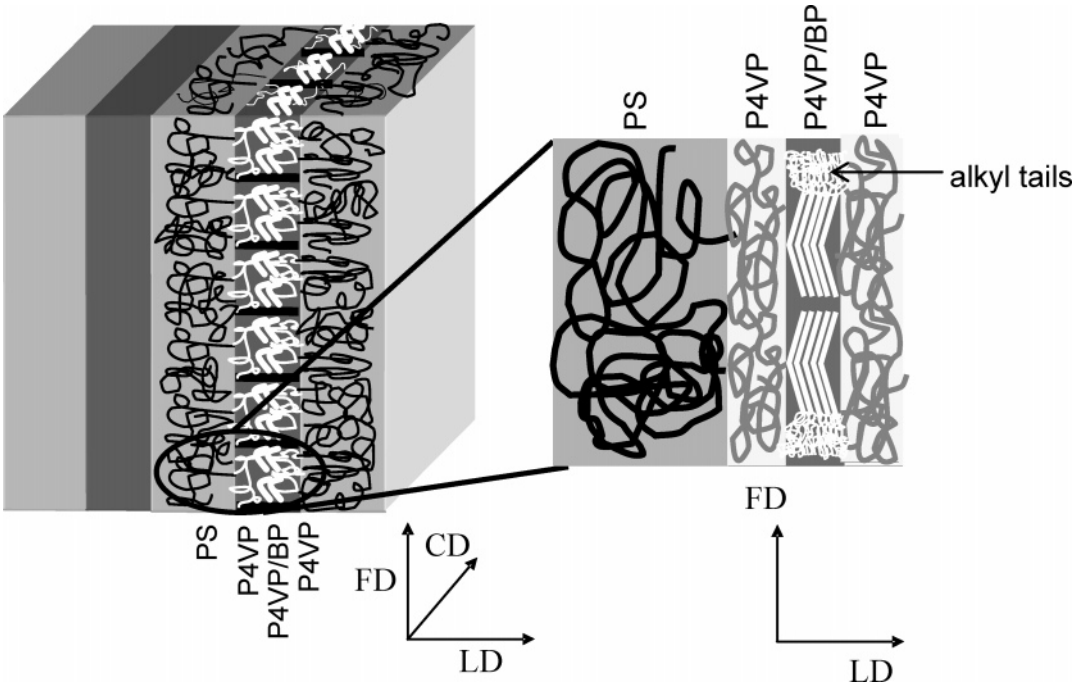

Figure 4. Schematic representation of the phase structures observed in PS−P4VP(BP)$_{0.1}$.

the FD/CD plane of the sample. White PS cylinders are clearly seen in the dark P4VP(BP)$_{0.2}$ matrix. On the basis of the X-ray and TEM observations, the phase structure of PS−P4VP(BP)$_{0.2}$ can be constructed as shown in Figure 7, which shows hexagonally packed PS cylinders (white) in the P4VP(BP)$_{0.2}$ matrix (dark). Increasing the concentration of BP in the BCP changes the P4VP(BP)$_{0.2}$ cumulative weight fraction to 0.73, leading to the transformation of the sample morphology from lamellae to hexagonally packed PS cylinders. In the P4VP(BP)$_{0.2}$ matrix, SmA_2 layers are oriented perpendicular to the BCP interface.

The orientation of the LC BCPs under flow has been carefully investigated for cylinder-forming side-chain LC BCPs.[49] Four possible structures were suggested by Thomas et al., including parallel−transverse, perpendicular−parallel, parallel−parallel, and transverse−perpendicular. In this notation, the first word represents the BCP cylinder orientation while the second one denotes the orientation of the LC layers. In their system, Thomas et al. observed parallel−transverse and transverse−perpendicular orientations depending upon whether the sample shearing temperature was in the isotropic phase or the LC phase of the LCPs, respectively. Thus, the authors were able to demonstrate the influence of the LC phase on the BCP morphology. Recently, Hammond et al. reported the phase structures of siloxane-functionalized side-chain LC−BCPs where the transverse orientation of the cylinders was retained even in the isotropic region of the LCP.[20] In our case, the orientation is perpendicular−parallel where the BCP cylinders are perpendicular to the FD/

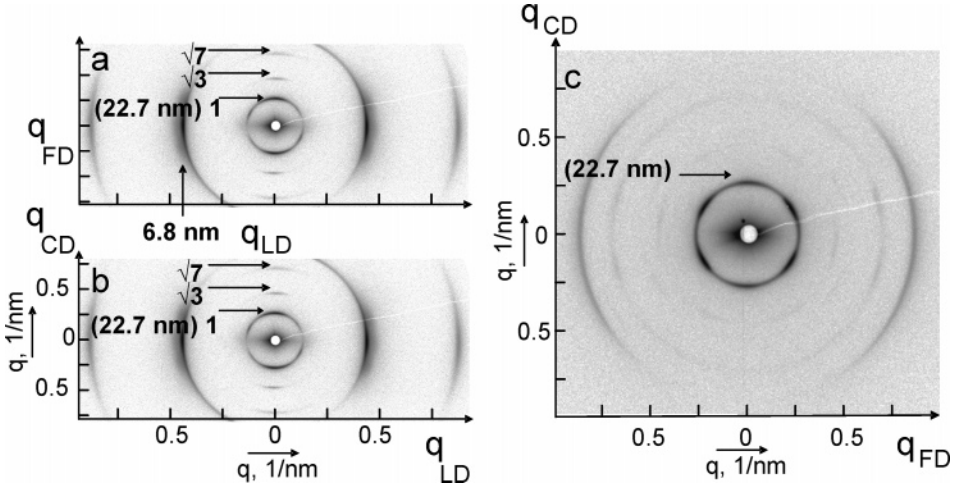

Figure 5. 2D small-angle X-ray scattering pattern of PS−P4VP(BP)$_{0.2}$ with the X-rays along the (a) constraint direction (CD), (b) flow direction (FD), and (c) loading direction (LD) as defined in Scheme 2.

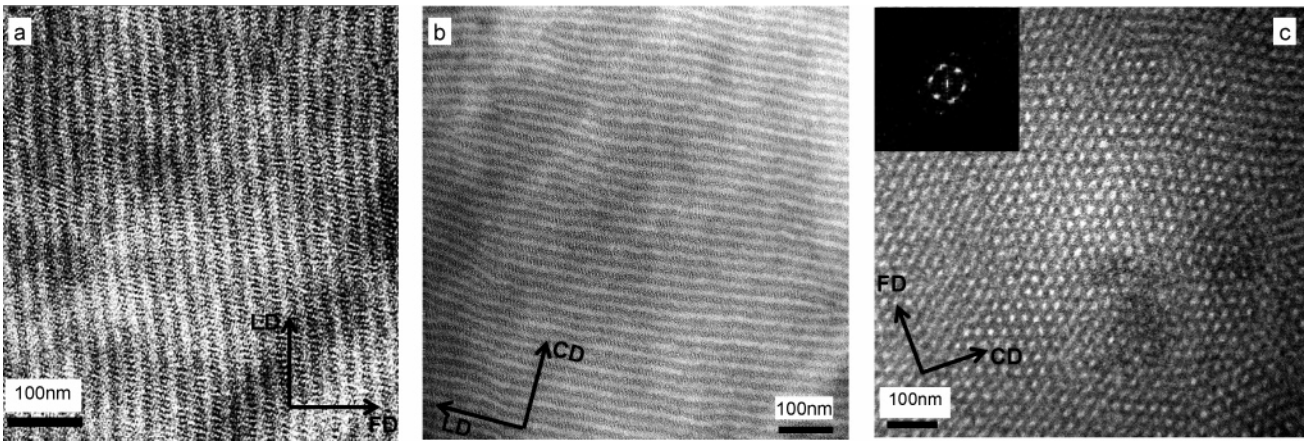

Figure 6. Transmission electron micrograph of PS−P4VP(BP)$_{0.2}$ showing the (a) flow/loading direction (FD/LD) plane, (b) constraint/loading direction (CD/LD) plane, and (c) flow/constraint direction (FD/CD) plane. (Inset on the left is the fast Fourier transform of the image along the FD/CD plane, which is similar to the SAXS pattern.)

CD plane and the smectic layer normal is parallel to the LD. In this case, BCP cylinders are in the least favorable orientation while the smectic layers are in their most favorable orientation. Formation of this unique orientation can be attributed to the fact that the present bent-core molecules possess longer mesogen groups compared to the previously reported systems. Therefore, under shear, smectic layers dictate the orientation of the system, and they assume a parallel orientation. Since homogeneous anchoring of the LCs on BCP cylinders is also important to minimize the defects of the system,[49] the PS cylinders were then forced to adopt a less favorable perpendicular orientation. These results show that the orientation of the LC BCP hierarchical nanostructures can be tuned by tailoring the molecular structure of the LCs.

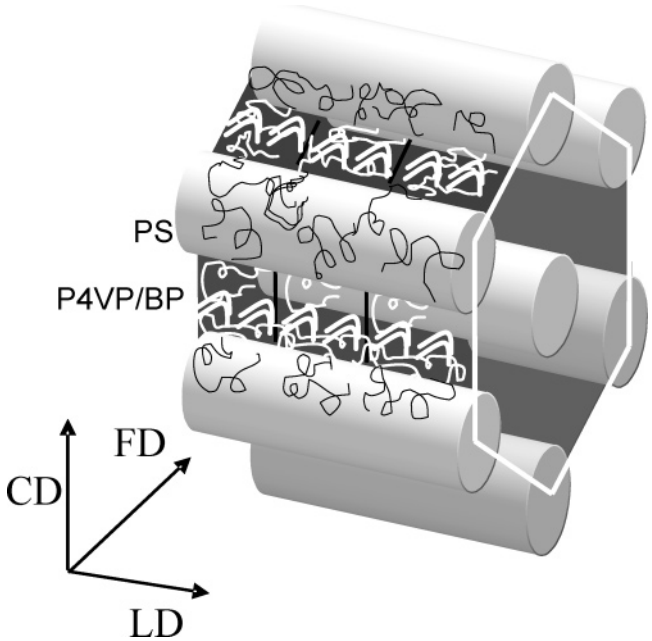

Figure 7. Schematic representation of the phase structures observed in PS−P4VP(BP)$_{0.2}$.

Conclusions

In summary, the phase structures of two PS-*b*-P4VP/BP blends were investigated. Hydrogen bonding between terminal −OH group of the bent-core molecule BP and nitrogen of P4VP led to the formation of the P4VP(BP)$_n$ complex. PS and P4VP-(BP)$_n$ underwent microphase separation and formed ordered structures in the 10−100 nm range, and within each P4VP-(BP)$_n$ domain, BP molecules undergo further phase separation to form layered stacks of ∼6.8 nm representing SmA_2 LC structures. Thus, structure-in-structure type of morphology was achieved due to hierarchical self-assembly at different length scales. When $n = 0.1$, LC smectic layers were formed within lamellar BCP domains where the SmA_2 layers were oriented perpendicular to the BCP interface. These samples exhibited

an increased long-range order and a decreased *d*-spacing compared to the original BCP. Because of the low BP content, further phase separation occurred between P4VP and P4VP/BP, leading to multiple (3) layers within each P4VP-rich domain. When $n = 0.2$, the morphology of the BCP transformed to a hexagonally packed cylindrical structure where PS cylinders are embedded in $P4VP(BP)_{0.2}$ matrix. Upon shearing, the PS cylinders are oriented perpendicular to the FD/CD plane, and smectic layer normal is oriented parallel to the LD, representing a perpendicular−parallel arrangement. This unique orientation was attributed to the relatively large mesogen groups of the present system.

Acknowledgment. This work was supported by the National Science Foundation (NSF CAREER award, DMR-0239415), ACS PRF, 3M, and DuPont. We also thank Prof. Karen Winey for the use of the ultramicrotomy equipment. K.K.T. thanks the Sigma Xi Grants-in-Aid of Research. X.H.W. and Q.F.Z. thank the National Natural Science Foundation of China (Nos. 20134010 and 20504002) for financial support. X.F.C. thanks the support from the Doctoral Program of the Higher Education Institution of Ministry of Education (20030001061). Synchrotron experiments were conducted at beamline X27C, NSLS, in Brookhaven National Laboratory supported by DOE.

References and Notes

(1) Park, C.; Yoon, J.; Thomas, E. L. *Polymer* **2003**, *44*, 6725−6760.
(2) Bates, F. S.; Fredrickson, G. H. *Annu. Rev. Phys. Chem.* **1990**, *41*, 525−557.
(3) Bates, F. S. *Science* **1991**, *251*, 898−905.
(4) Loo, Y.-L.; Register, R. A. Crystallization within block copolymer mesophases. In *Developments in Block Copolymer Science and Technology*; Hamley, I. W., Ed.; Wiley: New York, 2004; pp 213−244.
(5) Loo, Y.-L.; Register, R. A.; Ryan, A. J.; Dee, G. T. *Macromolecules* **2001**, *34*, 8968−8977.
(6) Zhu, L.; Calhoun, B. H.; Ge, Q.; Quirk, R. P.; Cheng, S. Z. D.; Thomas, E. L.; Hsiao, B. S.; Yeh, F.; Liu, L. *Macromolecules* **2001**, *34*, 1244−1251.
(7) Zhu, L.; Huang, P.; Chen, W. Y.; Ge, Q.; Quirk, R. P.; Cheng, S. Z. D.; Thomas, E. L.; Lotz, B.; Hsiao, B. S.; Yeh, F.; Liu, L. *Macromolecules* **2002**, *35*, 3553−3562.
(8) Hamley, I. W.; Castelletto, V.; Castillo, R. V.; Muller, A. J.; Martin, C. M.; Pollet, E. *Macromolecules* **2005**, *38*, 463−472.
(9) Gallot, B. *Prog. Polym. Sci.* **1996**, *21*, 1035−1088.
(10) Klok, H. A.; Lecommandoux, S. *Adv. Mater.* **2001**, *13*, 1217−1229.
(11) Lee, M.; Cho, B. K.; Zin, W. C. *Chem. Rev.* **2001**, *101*, 3869−3892.
(12) Poser, S.; Fischer, H.; Arnold, M. *Prog. Polym. Sci.* **1998**, *23*, 1337.
(13) Anthamatten, M.; Zheng, W. Y.; Hammond, P. T. *Macromolecules* **1999**, *32*, 4838−4848.
(14) Mao, G.; Wang, J.; Clingman, S. R.; Ober, C. K.; Chen, J. T.; Thomas, E. L. *Macromolecules* **1997**, *30*, 2556−2567.
(15) Olsen, B. D.; Segalman, R. A. *Macromolecules* **2006**, *39*, 7078−7083.
(16) Stupp, S. I. *Curr. Opin. Colloid Interface Sci.* **1998**, *3*, 20−26.
(17) Li, C. Y.; Tenneti, K. K.; Zhang, D.; Zhang, H.; Wan, X.; Chen, E.; Zhou, Q.; Avila-Orta, C.; Sics, I.; Hsiao, B. *Macromolecules* **2004**, *37*, 2854−2860.
(18) Tenneti, K. K.; Chen, X. F.; Li, C. Y.; Wan, X.; Zhou, Q. F.; Sics, I.; Hsiao, B. *J. Am. Chem. Soc.* **2005**, *127*, 15481−15490.
(19) Chen, J. T.; Thomas, E. L.; Ober, C. K.; Mao, G. P. *Science* **1996**, *273*, 343−346.
(20) Verploegen, E.; McAfee, L. C.; Tian, L.; Verploegen, D.; Hammond, P. T. *Macromolecules* **2007**, *40*, 777−780.
(21) Brandys, F. A.; Bazuin, C. G. *Chem. Mater.* **1996**, *8*, 83−92.
(22) Ikkala, O.; Ruokolainen, J.; ten Brinke, G.; Torkkeli, M.; Serimaa, R. *Macromolecules* **1995**, *28*, 7088−7094.
(23) Nandan, B.; Lee, C.-H.; Chen, H.-L.; Chen, W.-C. *Macromolecules* **2005**, *38*, 10117−10126.
(24) Ruokolainen, J.; Tanner, J.; ten Brinke, G.; Ikkala, O.; Torkkeli, M.; Serimaa, R. *Macromolecules* **1995**, *28*, 7779−7784.
(25) Valkama, S.; Lehtonen, O.; Lappalainen, K.; Kosonen, H.; Castro, P.; Repo, T.; Torkkeli, M.; Serimaa, R.; ten Brinke, G.; Leskelae, M.; Ikkala, O. *Macromol. Rapid Commun.* **2003**, *24*, 556−560.
(26) Valkama, S.; Ruotsalainen, T.; Kosonen, H.; Ruokolainen, J.; Torkkeli, M.; Serimaa, R.; ten Brinke, G.; Ikkala, O. *Macromolecules* **2003**, *36*, 3986−3991.
(27) Ikkala, O.; ten Brinke, G. *Chem. Commun.* **2004**, 2131−2137.
(28) Ruokolainen, J.; Makinen, R.; Torkkeli, M.; Makela, T.; Serimaa, R.; ten Brinke, G.; Ikkala, O. *Science* **1998**, *280*, 557−560.
(29) Ruokolainen, J.; ten Brinke, G.; Ikkala, O. *Adv. Mater.* **1999**, *11*, 777−780.
(30) Fahmi, A. W.; Braun, H. G.; Stamm, M. *Adv. Mater.* **2003**, *15*, 1201−1204.
(31) Sidorenko, A.; Tokarev, I.; Minko, S.; Stamm, M. *J. Am. Chem. Soc.* **2003**, *125*, 12211−12216.
(32) Kato, T.; Mizoshita, N.; Kanie, K. *Macromol. Rapid Commun.* **2001**, *22*, 797−814.
(33) Kato, T.; Mizoshita, N.; Kishimoto, K. *Angew. Chem., Int. Ed.* **2006**, *45*, 38−68.
(34) Chen, X.; Tenneti, K. K.; Li, C. Y.; Bai, Y.; Wan, X. H.; Fan, X.; Zhou, Q. F.; Rong, L.; Hsiao, B. S. *Macromolecules* **2007**, *40*, 840−848.
(35) Coleman, D. A.; Fernsler, J.; Chattham, N.; Nakata, M.; Takanishi, Y.; Korblova, E.; Link, D. R.; Shao, R. F.; Jang, W. G.; Maclennan, J. E.; Mondainn-Monval, O.; Boyer, C.; Weissflog, W.; Pelzl, G.; Chien, L. C.; Zasadzinski, J.; Watanabe, J.; Walba, D. M.; Takezoe, H.; Clark, N. A. *Science* **2003**, *301*, 1204−1211.
(36) Niori, T. S. T.; Watanabe, J.; Furukawa, T.; Takezoe, H. *J. Mater. Chem.* **1996**, *6*, 1231−1233.
(37) Pelzl, G.; Diele, S.; Weissflog, W. *Adv. Mater.* **1999**, *11*, 707−724.
(38) Pelzl, G.; Wirth, I.; Weissflog, W. *Liq. Cryst.* **2001**, *28*, 969−972.
(39) Shen, D.; Pegenau, A.; Diele, S.; Wirt, I.; Tschierske, C. *J. Am. Chem. Soc.* **2000**, *122*, 1593−1601.
(40) Walba, D. M.; Korblova, E.; Shaob, R.; Clark, N. A. *J. Mater. Chem.* **2001**, *11*, 2743−2747.
(41) Hasegawa, H.; Hashimoto, T.; Kawai, H. *Macromolecules* **1985**, *18*, 67−78.
(42) Matsen, M. W.; Bates, F. S. *Macromolecules* **1996**, *29*, 1091−1098.
(43) Chen, X.; Tenneti, K. K.; Li, C. Y.; Bai, Y.; Zhou, R.; Wan, X.; Fan, X.; Zhou, Q. F. *Macromolecules* **2006**, *39*, 517−527.
(44) Hashimoto, T.; Tanaka, H.; Hasegawa, H. *Macromolecules* **1990**, *23*, 4378−4386.
(45) Matsushita, Y.; Mori, K.; Saguchi, R.; Nakao, Y.; Noda, I.; Nagasawa, M. *Macromolecules* **1990**, *23*, 4313−4316.
(46) Tanaka, H.; Hasegawa, H.; Hashimoto, T. *Macromolecules* **1991**, *24*, 240−251.
(47) Torikai, N.; Takabayashi, N.; Noda, I.; Koizumi, S.; Morii, Y.; Matsushita, Y. *Macromolecules* **1997**, *30*, 5698−5703.
(48) Winey, K. I.; Thomas, E. L. F. L. J. *Macromolecules* **1991**, *24*, 6182−6188.
(49) Osuji, C.; Chen, J. T.; Mao, G.; Ober, C. K.; Thomas, E. L. *Polymer* **2000**, *41*, 8897−8907.

MA070721J